Electrical characterization and performance limits of a flexible cable

by A. Deutsch
D. W. Dranchak
G. Arjavalingam
C. W. Surovic
J. K. Tam
G. V. Kopcsay
J. B. Gillett

The electrical performance of a flexible-cable test structure is characterized from low frequencies up to 25 GHz. The experimental results are used to develop and refine models which describe the performance of such cables, with particular emphasis on the contribution of dielectric and resistive losses, including skin effect. The capability of triplate flexible cables to provide high-bandwidth connections over long lengths is investigated with the models developed. A triplate design is chosen because it offers high density, limited crosstalk, no loss through radiation, and relatively inexpensive fabrication. Bit rates of 100 Mb/s–1 Gb/s are considered for propagation over lengths up to 250 cm. The paper highlights the performance-limiting factors through realistic examples, including the contribution of interfaces to other interconnection structures.

1. Introduction

Metallized flexible films are being used extensively as electronic interconnections in a variety of applications. In consumer products they are primarily used because of their low cost, while in compact devices, such as hand-held calculators and disk drives, they are used for their small size. In printers and copiers they provide a large number of connections while also accommodating the smooth mechanical movement of electrically active components [1, Ch. 15]. Most flexible cables consist of Kapton™ or Upilex™ ribbons which are metallized on one or both sides. The same basic technology is the basis of the tape-automated-bond (TAB) structures now being used as single-chip carriers in some computer applications. Examples of these include the flipped-TAB-carrier (FTC) module found in the Fujitsu VP2000 [2] and NEC SX-3 [3] series of supercomputers. More recently, a similar structure has been proposed as the first-level package for a 125-MHz microprocessor [4]. Since fast rise-time signals must be propagated with controlled impedance and crosstalk (coupled noise), such high-performance applications require metallization on both sides of the dielectric film. Usually, though not always, one side contains the signal wires, while the other is a ground plane. Structures with similar cross-sectional designs have also been developed for high-density connector applications [5] and are now commercially available [6]. They are expected to replace more conventional pluggable connectors, providing surface-to-surface electrical contact.

In large computer complexes a variety of cables are used to connect the central processing units to one another, to the input/output (I/O) subsystems, and to mass storage devices. For example, in Hitachi M-880 computers, coaxial cables with 1.27-mm pitch transfer signals between two large-scale processor boards with short propagation delays (3.8 ns/m) [7]. In a similar application, bundles of 0.98-mm-diameter, 1.27-mm-pitch coaxial cables provide interprocessor connectivity in NEC ACOS 3900 computers with 3.6-ns/m delay [8]. Ribbons of 1.88-mm-diameter, 2.54-mm-pitch coaxial cables containing a low-dielectric-constant polytetrafluoroethylene (PTFE) insulator (ε_r = 1.3) are commercially available [1, Ch. 14] and can be used to transmit 10-ns-wide pulses over lengths of 5–10 m [9]. However, coaxial cable assemblies are not inexpensive, costing about $5–10 per signal line [10]. An alternative is to use flexible cables containing several signal and ground connections on the same ribbon. Since they can be fabricated by batch processing, the cost per connection is expected to be much lower. Such flexible cables are also now commercially available [11] and are being considered for high-performance applications. An example is the 55-cm-long Kapton-based cable, with about 20 connections per cm of width, which was developed to provide the I/O communication in a Josephson junction computer [12]. That cable was expected to support a 300-ps rise-time signal with little signal degradation. Similar high-density high-bandwidth cables will continue to be needed, especially in the massively parallel computer systems currently under development.

In this paper the electrical performance of a flexible circuit test vehicle is completely characterized, and with this knowledge, the capability of such cables to provide high-bandwidth connections over long lengths is predicted. Following a brief description of the overall design and fabrication of the test structure, its characterization by time-domain measurement techniques is presented. In particular, a novel short-pulse propagation technique is used to measure the frequency-dependent complex propagation constant and impedance of a particular transmission-line design. These results, together with low-frequency capacitance and resistance measurements, are used to refine the electrical models which describe the performance of the flexible cable. In addition, we discuss the effect of process tolerances on these models. The ability of the cable to propagate fast rise-time pulses is investigated experimentally with the transmission of 15- and 35-ps rise-time pulses. Its use in realistic applications is simulated with the transmission of 200-ps rise-time ± 500-mV amplitude signals. Maximum usable lengths and the expected crosstalk noise are determined from these simulations. A triplate flexible cable with superior electrical characteristics is recommended for applications with the most stringent requirements. Finally, the application of such a cable to connect a chip carrier to a board is simulated.

2. Test vehicle design

The different cross-sectional designs of flexible cables, currently available or under development, are shown schematically in **Figure 1**. Figure 1(a) is a coplanar waveguide structure in which the signal lines are surrounded by reference conductors. While this design has the fewest layers and provides the highest packing density, it requires very accurate control of line-to-line separation. Large processing variations, inherent in inexpensive fabrication techniques, would result in large tolerances for the electrical characteristics of this design. Figures 1(b) and 1(c) use two metal layers. The reference for the transmission lines is either a solid ground plane [Figure 1(b)] or a pseudo-coaxial configuration, as shown in Figure 1(c), with both a ground plane and ground conductors on either side of the signal line. For the same signal-line pitch, the latter design provides somewhat better shielding of the signal lines than the design of Figure 1(b). However, it can result in increased capacitive coupling between lines if the ground conductors are not reliably connected to the bottom plane. The microstrip design of Figure 1(b), which is popular, has the lowest packing density, since it has the largest crosstalk for a particular line-to-line separation.

The structures in Figures 1(a)–1(c) can all be designed to satisfy most electrical requirements such as impedance, dispersion, and coupling. However, they will lose energy through radiation, especially if the length becomes substantial. Moreover, they are not closed-transmission-line systems, and stacking them can affect the line impedance while also introducing additional coupled noise. The best electrical configuration is shown in Figure 1(d), a triplate structure composed of three metal layers. In this case, since the signal lines are shielded by two planes, there is no radiation even for very long cables. While the connection density is better than for Figure 1(b), the fabrication sequence is somewhat more complex. In fact, the microstrip design of Figure 1(b) is first fabricated, and then covered through lamination with a Kapton film having the top ground plane only. The characteristics of the triplate structure are mainly determined by the line width W, separation S, and Kapton thickness h_1. The top

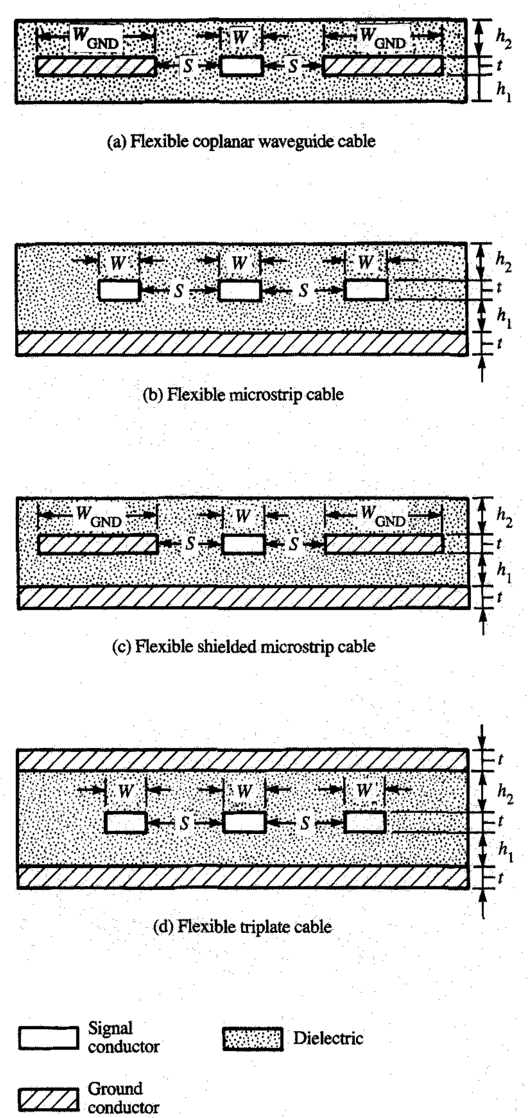

Figure 1

Example cross-sectional designs for flexible cables: (a) coplanar waveguide with one metal layer, (b) microstrip structure using two metal layers, (c) shielded microstrip configuration with ground plane and ground conductors, (d) triplate structure with top and bottom ground planes. W is line width, S is separation, h_1 and h_2 are Kapton layer thicknesses, and t is metal thickness.

Kapton layer thickness h_2 is sometimes much larger than h_1 and then does not need tight dimensional control, thus keeping its processing fairly simple.

A top view of the test vehicle which is the subject of this paper is shown in **Figure 2**. The overall size of the sample, which contains several different experiments, is 16 × 18 cm. Electrical measurements on transmission-line structures which have the cross-sectional designs of Figures 1(b) (microstrip) or 1(c) (shielded microstrip) are presented in Sections 4 and 5. A 50-μm-thick Kapton sheet was used as the starting material, on which lines of various designs and dimensions were fabricated with the procedure described in the next section. The transmission lines were 14.3 cm in length, and the signal conductors had a range of widths from 50 μm to 200 μm.

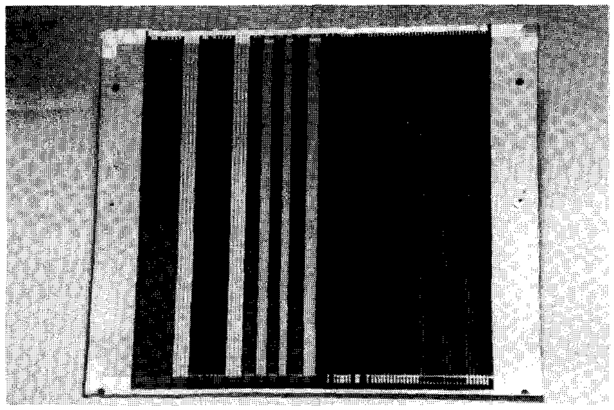

Figure 2

Top view of 16 × 18-cm test vehicle which incorporates a variety of flexible cable designs. The lines are 14.3 cm long.

3. Fabrication

Most flexible cables of the type discussed here use Kapton as the dielectric insulator. Kapton, which is made of poly(N, N–bis(phenoxyphenyl)–pyromellitimide) (PMDA–ODA) [13], has a dielectric constant of 3.5, and was measured to have low dielectric loss [14]. Worst-case specifications from vendors usually indicate loss tangent values of about 0.0036 at 1 kHz. Most dielectric measurements, other than the newly developed COMITS technique of [14], are carried out at discrete frequencies, and over limited bandwidths [15]. One specific advantage is that Kapton does not thermally degrade except at high temperatures (>350°C). Rolls of Kapton with a range of thicknesses from about 12.5 μm to 250 μm are commercially available. Our test structure was fabricated with the following procedure: A 50-μm-thick sheet was completely metallized on one side to define the ground plane. Holes for layer-to-layer vias were mechanically punched, and a metallic seed layer for plating was deposited on the unmetallized side. The line designs were photolithographically defined and metallized by plating. The vias were plated at the same time as the lines. Adhesive layers between the polymer and copper lines were not needed. Following removal of the photoresist mask, the seed layer was etched away where it was not desired. Protective Kapton sheets were laminated to both sides of the metallized film over the entire surface, except for the end pads, with a layer of acrylic adhesive.

4. Characterization of shielded microstrip lines

The complex propagation properties of transmission-line structures with the shielded microstrip configuration of Figure 1(c) were characterized with the recently developed short-pulse propagation technique [16]. Briefly, a short electrical pulse is launched onto identical transmission lines of lengths l_1, l_2. The attenuated and dispersed pulse waveforms at the ends of the lines are recorded with a sampling oscilloscope. Time windowing is used to extract the forward-traveling wave only and to eliminate any unwanted reflections. The two waveforms are numerically Fourier transformed. The ratio of these complex Fourier spectra then yields the frequency-dependent complex propagation constant $\Gamma(f)$,

$$\alpha(f)+j\beta(f) = -\frac{1}{l_1-l_2}\ln\frac{A_1(f)}{A_2(f)}+j\frac{\Phi_1(f)-\Phi_2(f)}{l_1-l_2}, \tag{1}$$

where $\alpha(f)$ and $\beta(f)$ are the frequency-dependent attenuation and phase constant, respectively. A_i, Φ_i ($i = 1, 2$) are the amplitude and phase of the Fourier transforms corresponding to lines l_1 and l_2, with $l_1 > l_2$. For transmission lines in which dielectric dispersion and loss are small, the complex impedance $Z_0(f)$ is obtained from [16]:

$$Z_0 = \frac{\beta}{\omega C} - j\frac{\alpha}{\omega C}, \tag{2}$$

where C is the line capacitance per unit length.

In **Figure 3** we show the schematic layout of the shielded microstrip lines that were characterized with the short-pulse propagation technique. For the 14.26-cm-long lines, the input signal was launched at point A, while the transmitted signal was probed at point B. The coplanar ground conductors were used to make ground contact. They connected to the bottom ground plane through several 200-μm-diameter vias, as shown in Figure 3. A short "zero-delay" transmission line was created by mechanically cutting an isolated 60-μm (l_2) length of line (as shown in Figure 3) and probing it at points C and D. Thus, the difference in line lengths was 14.254 cm. A cross-sectional optical micrograph of a sample similar to that of Figure 3 is shown in **Figure 4(a).**

A 35.4-ps-wide pulse was obtained by differentiating the step source of a 20-GHz sampling oscilloscope. A commercially available passive impulse-forming network* was used as the differentiator. As shown in **Figure 5**, the short electrical pulse was launched onto the sample with the high-speed bird's-beak coaxial probes described in [17]. The pulse waveforms recorded at the ends of the lines are shown in **Figure 6.** While the short transmission line does not disperse the input pulse in any detectable way, the

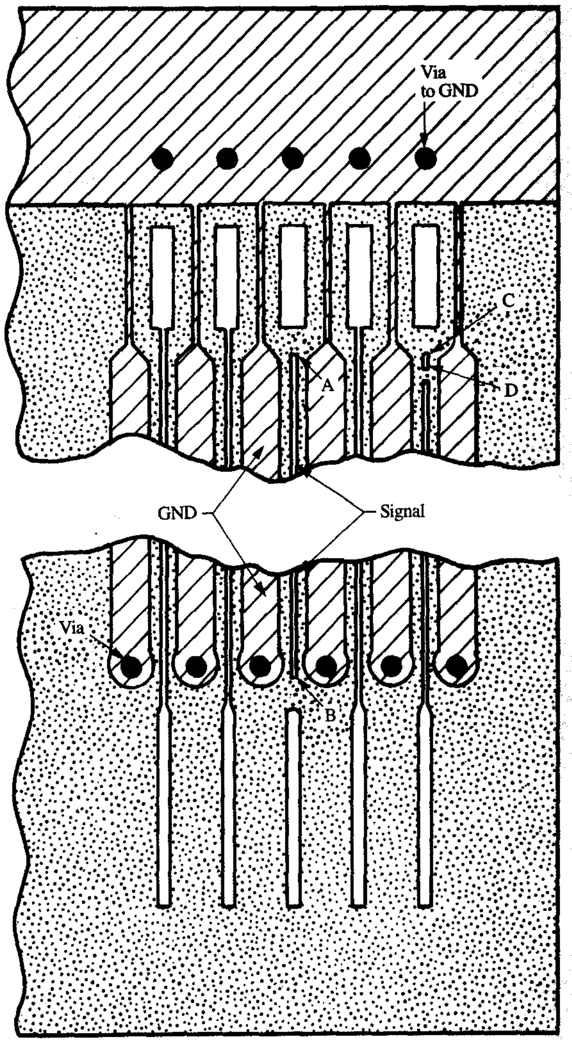

Figure 3

Schematic representation of the shielded microstrip test cell showing the probing of the long line (l_1 = 14.26 cm) at points A and B, and of the short line (l_2 = 60 μm) at points C and D.

* Impulse Forming Network Model 5208 made by Picosecond Pulse Laboratories, P.O. Box 44, Boulder, CO 80306.

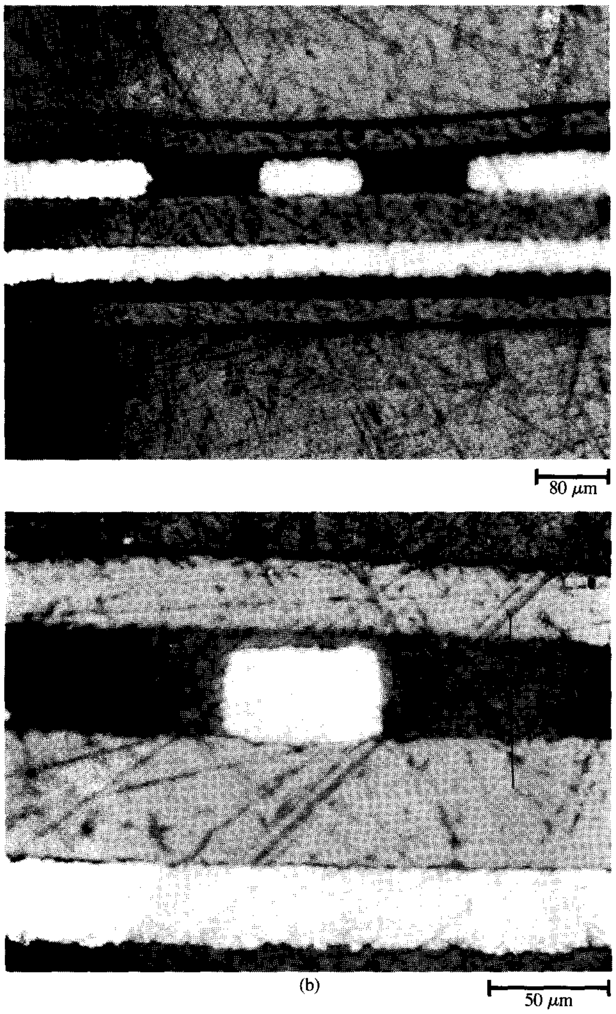

Figure 4

Cross-sectional optical micrographs of portions of the test vehicle: (a) shielded microstrip configuration with 80.7-μm-wide signal line surrounded by two 473-μm-wide ground conductors and (b) microstrip structure with 55.7-μm-wide signal line. Both designs have a 57-μm-thick Kapton overcoat.

pulse at the output of the long line is clearly attenuated and has a full width at half maximum of 45.6 ps. A set of computer routines developed internally was used to extract the frequency-dependent attenuation coefficient and phase constant up to 25 GHz, as described by Equation (1). These results are shown as points in **Figure 7**. The frequency dependence of the capacitance is usually dominated by the dispersion of the dielectric constant, which is very small for low-loss dielectrics. It is shown in [14] that the dielectric constant of polyimide is almost constant well beyond the 25-GHz upper limit of the results of Figure 7.

The frequency-dependent transmission-line characterization described above is complemented with low-frequency capacitance and resistance measurements. Together with dimensional measurements, these results are used to develop and refine the models which describe the electrical behavior of the flexible cables. A capacitance bridge (Boonton Electronics Model 72BD) operating at 1 MHz was used for the capacitance measurements, while resistance values were obtained with a multimeter (Hewlett Packard Digital Voltmeter Model 3456A). The measured complex propagation constant and the per-unit-length capacitance measured at 1 MHz were used to obtain the complex impedance shown in **Figure 8** [16].

The physical dimensions of the samples were determined through a variety of techniques. Line widths were measured using both a stylus profilometer and a high-magnification measurement microscope. The line metal thicknesses were also measured with the profilometer, and later confirmed by cross-sectional microscopy on a sister sample fabricated at the same time. Portions of the actual sample characterized were also cross-sectioned. Many of the dimensions were found to be uniform, not only along the length of the lines, but also from sample to sample. By using Figure 1(c) as reference, the top width of the line was measured to be 80.7 ± 2.7 μm. The cross-sectional micrograph of Figure 4(a) shows that the bottom width is actually narrower by a few micrometers, a fact which affects its ac electrical behavior. The metal thickness (t) was 32.7 ± 1.2 μm, while the dielectric thicknesses were $h_1 = 50 \pm 1$ μm and $h_2 = 57 \pm 4.2$ μm, respectively. The separation between the signal conductor and the coplanar ground conductors (S) was 132 ± 3.3 μm, while the ground conductor width W_{GND} was 473 ± 5.0 μm.

The electrical properties of the shielded microstrip transmission line were modeled using the procedure described in [18]. First, the Kapton dielectric constant ε_r was determined to be 3.27 by means of capacitance measurements on a parallel-plate capacitor made from the flexible cable. A line cross section close to that observed in cross-sectional microscopy was employed in a low-frequency 2D static modeling program [19] which predicted a per-unit-length capacitance of 1.18 pF/cm. The corresponding measured value was 1.13 pF/cm. The measured line resistance of 0.08 Ω/cm gave a resistivity for copper of 1.95 microhm-centimeters ($\mu\Omega$-cm).

The frequency-dependent attenuation and phase constant were calculated with the technique described in [18]. For these calculations, the line was assumed to have a rectangular cross section with 73-μm width in order to accommodate the limitations of the modeling programs [20]. The modeled values are shown as lines in Figure 7. The best agreement with measured values was obtained when the Kapton dielectric was assumed to have a loss tangent (tan δ) of 0.008. The largest differences between the measured and modeled values of attenuation and phase constant were 2% and 7.3%, respectively. The modeled

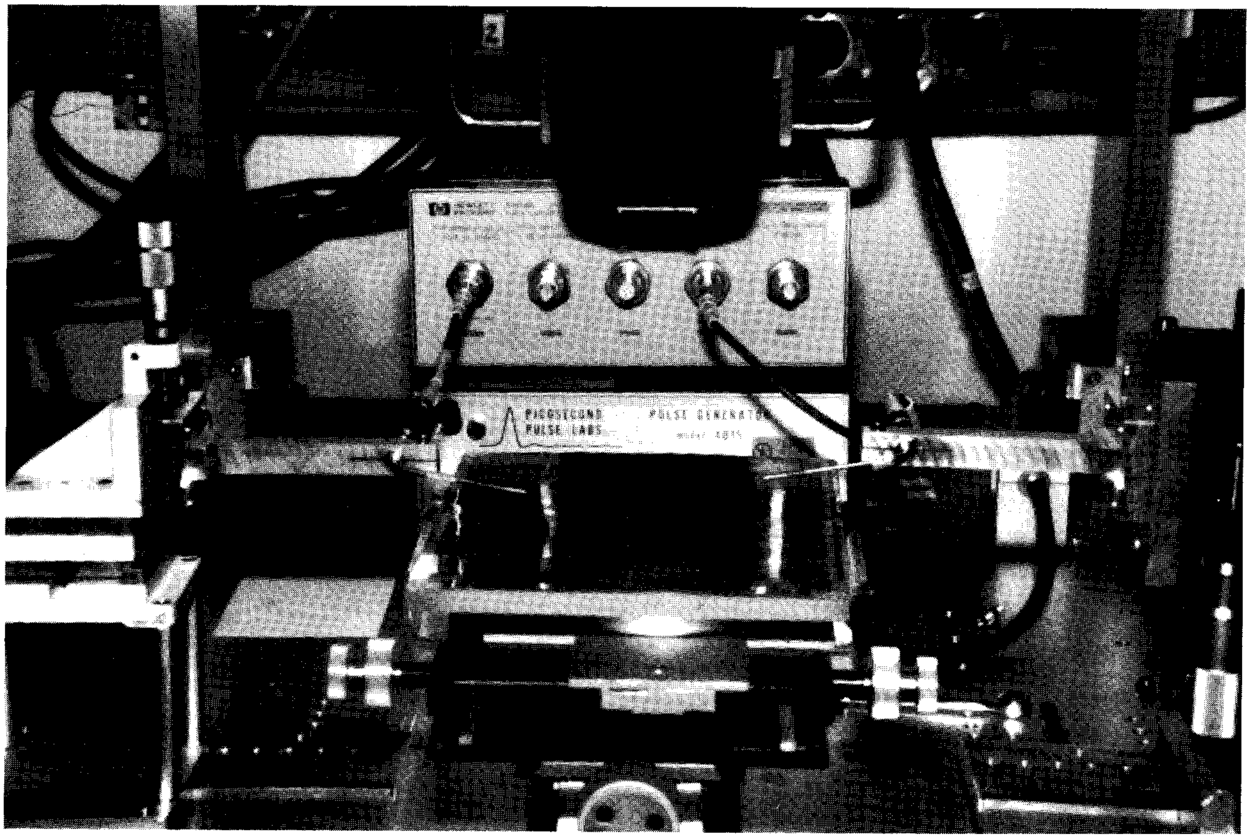

Figure 5

Experimental setup showing the test vehicle of Figure 2 being characterized with the 20-GHz sampling oscilloscope. The step source of the oscilloscope is converted to a 35-ps-wide pulse by an in-line passive differentiator. Signals are input to and output from the sample under test with custom-made "bird's beak" coaxial probes [17].

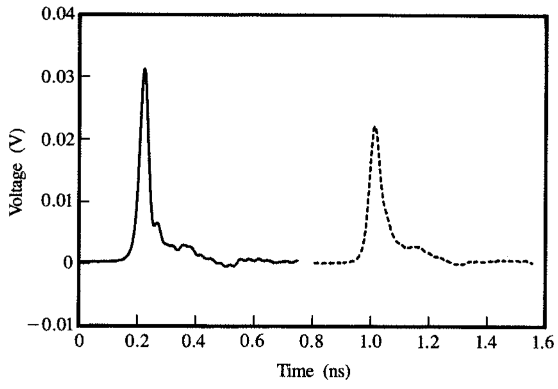

Figure 6

Pulse waveforms measured at the ends of the 14.26-cm-long (dashed trace) and the 60-μm-long (solid trace) transmission lines of Figure 5. The pulse widths are 45.6 and 35.4 ps, respectively. The dc resistance (R_{dc}) of the lines is 0.08 Ω/cm.

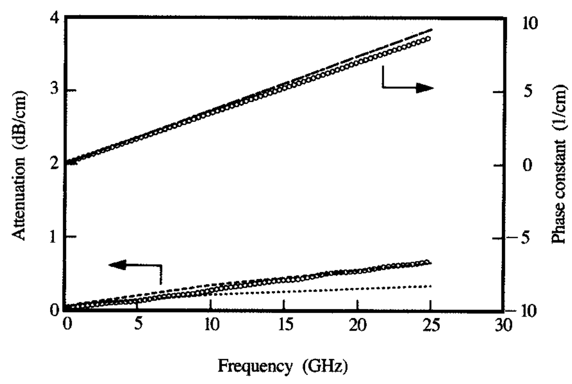

Figure 7

Phase constant $\beta(f)$ and attenuation coefficient $\alpha(f)$ obtained experimentally (dots) and modeled with loss tangent, $\tan \delta = 0.0$ (dotted trace), and $\tan \delta = 0.008$ (dashed trace).

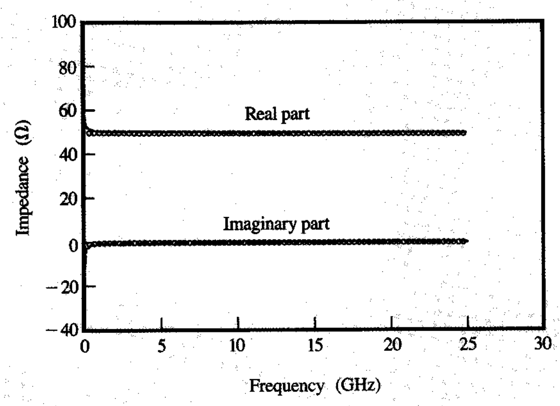

Figure 8

Real and imaginary parts of the characteristic impedance. Points are experimentally obtained with the short-pulse propagation technique; dashed lines are predictions of modeling. The modeled values of impedance for tan δ = 0.0 and tan δ = 0.008 are almost identical.

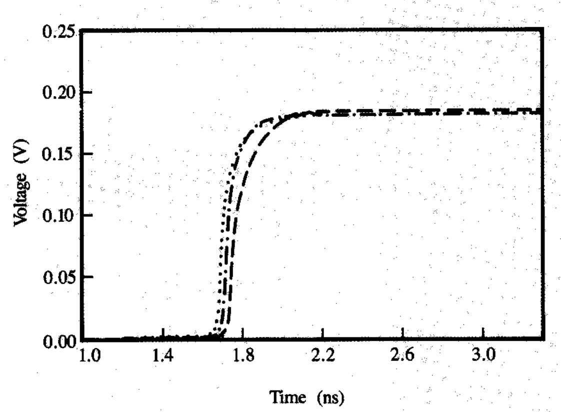

Figure 9

Step function response at the end of a 14.26-cm-long shielded microstrip line having the cross section of Figure 4(a). The dotted line is a TDT waveform measured with the 20-GHz oscilloscope. Simulated waveforms using modeled parameters (dashed line) and parameters determined through measurement with the short-pulse technique (dotted–dashed line) are also shown.

value of attenuation with tan $\delta = 0$ is also shown in Figure 7 and is clearly not the best description. Nevertheless, it should be emphasized that the measured loss coefficient of the structure is very small (<1.0 dB/cm at 25 GHz).

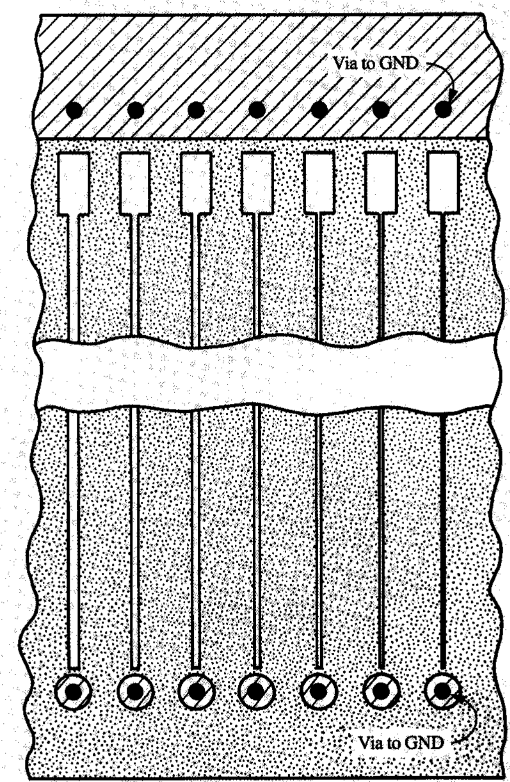

Figure 10

Schematic representation of the test site with microstrip lines having design widths of 50–200 μm. A via having a 203-μm (8-mil) diameter connects the top ground pads to the bottom ground plane.

While skin effect becomes significant for these lines around 0.4 GHz, the low resistance and wide line width are responsible for the low resistive attenuation. Moreover, the loss tangent of 0.008 produces very small attenuation due to dielectric loss. Therefore, the assumptions made in deriving Equation (2) still hold. The theoretically predicted complex impedance values are presented along with the measured values in Figure 8. The discrepancy is less than 1.1%.

The propagation of logic-like step functions on this flexible cable was simulated using a transient circuit simulator [21]. Both the modeled parameters and those determined through measurements were input to the simulation. These results are compared with actual measurements in **Figure 9**, with generally excellent agreement. The comparison between TDR (time domain reflection) measurements and results of the corresponding simulations is also excellent. It should be clear from the above discussion that the short-pulse propagation technique provides a simple and inexpensive means of accurately characterizing transmission lines with negligible dielectric attenuation. Though not a factor for the flexible cables, it also provides a more accurate means of determining the characteristic impedance of resistive lines compared with TDR measurements [16].

In summary, in this section we have used measurements to determine accurate values for dielectric constant and loss tangent. The generally excellent agreement between theoretically predicted and measured electrical parameters gives us confidence in the modeling procedure. The same modeling procedure is employed in later sections to predict the limits of performance of flexible cables with different designs and to determine a range of applications for which they are suitable.

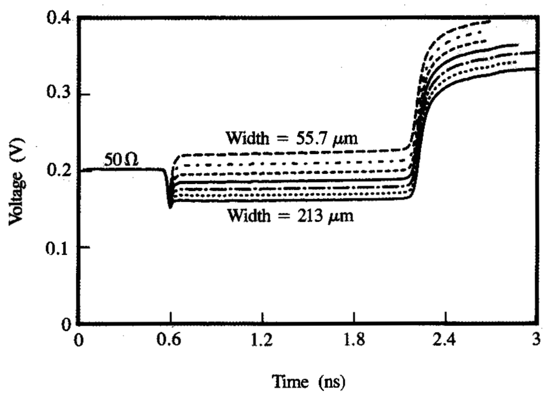

Figure 11

Measured TDR response of the 14.3-cm-long microstrip lines of Figure 10. The actual line widths measured with a microscope, in μm, are 55.7, 82.5, 107.5, 134.5, 161.3, 187.6, and 212.8.

5. Characterization of 50–200-μm-wide microstrip lines

Measurements and modeling were also carried out on a microstrip [Figure 1(b)] test cell. The layout is shown in **Figure 10**. A typical cross section for the 50-μm line is shown in Figure 4(b). The lines have a large rectangular pad at one end, and a 0.63-mm-diameter circular pad at the other end. Although the line widths were designed to be 50.8, 76.2, 101.6, 127.0, 152.4, 177.8, and 203.2 μm (2, 3, 4, 5, 6, 7, and 8 mil), the samples we received had line widths of 55.7, 82.5, 107.5, 134.5, 161.3, 187.6, and 212.8 μm (2.2, 3.2, 4.2, 5.3, 6.4, 7.4, and 8.4 mil). The small difference (~10%) between design and as-fabricated line widths implies reasonably well controlled fabrication processes. Because all the lines had the same separation (h_1) from ground, the characteristic impedance varied from 33.2 to 60.8 Ω.

TDR and TDT (time domain transmission) measurements were performed on these lines with the 20-GHz sampling oscilloscope. **Figure 11** shows the TDR

Table 1 Microstrip test structure. Measured and calculated line resistance R, capacitance C, propagation delay τ, and characteristic impedance Z_0. Lines are 14.3 cm long and 55.7–212.8 μm wide, and have the microstrip structure of Figure 1(b) and layout shown in Figure 10. TDR results are shown in Figure 11; the line capacitance was calculated with the measured dielectric constant ε = 3.27 and includes the test pad contribution of C = 0.59 pF.

W (μm) (mils)	R_{meas} (Ω/cm)	C_{meas} (pF)	C_{cal} (pF)	τ_{meas} (ps/cm)	τ_{cal} (ps/cm)	Z_{0meas} (Ω)	Z_{0cal} (Ω)
55.7 2.2	0.09	14.89	15.05	56.5	57.1	60.8	59.0
82.5 3.2	0.064	16.99	17.60	56.6	56.7	53.2	50.1
107.5 4.2	0.047	19.18	19.30	56.7	56.8	46.9	45.6
134.5 5.3	0.037	21.00	21.54	56.8	56.8	42.3	40.7
161.3 6.4	0.03	23.20	23.87	56.9	56.8	38.9	36.6
187.6 7.4	0.026	25.30	26.29	57.0	56.8	35.7	33.2
212.8 8.4	0.022	27.30	28.50	57.2	56.8	33.2	30.6

l = 14.3 cm, ε = 3.27, C_{pad} = 0.59 pF.

traces for the seven lines. A large capacitive discontinuity due to the large input pad ($C = 0.59$ pF) is present at the beginning of the waveforms. The measured and calculated characteristic impedance (Z_0) values are given in **Table 1**. The agreement is fairly good, given that TDR impedance measurements have an accuracy of 5–10%. The measured and calculated line capacitance values agree within 4.5%. Since the accuracy of capacitance measurements is believed to be around ±1% in this case, the discrepancy is likely due to nonuniformity in the line cross sections. It should be noted that the calculated values of capacitance C_{cal}, propagation delay τ_{cal}, and characteristic impedance Z_{0cal} take into account the fact that a 13.9-cm length of every line is covered with the protective Kapton covercoat. A short length of each line (0.384 cm) and the pads for signal and ground contact are left exposed to provide access for probing.

As can be seen from Table 1, the lines have low dc resistance: namely, 0.022–0.09 Ω/cm. It should be noted that even at 10 GHz, the attenuation is calculated to be only 0.216–0.36 dB/cm (with $\tan \delta = 0.008$). For the 14.3-cm length, this translates to only 3–5 dB in loss. The rise-time dispersion (not shown) observed in TDT with the 35-ps step source was practically the same for all the widths considered. Also, the measured and calculated (without loss) propagation delays of the 50% level, shown in Table 1, agreed to within 1.7%. The measured values were nearly equal for all seven cases. Frequency-dependent losses will be shown to limit signal propagation on much longer lines. These losses affect high-frequency components the most, resulting in the rounding of the upper part of the transition and, thus, a slower rise time [18]. For the 14.3-cm-long line, our calculations predict that dielectric losses increase the rise time by 38 ps over the loss-free case, for an input rise time of 35 ps. The actual output rise time was 204 ps. As discussed in the next section, the microstrip structures were very useful in analyzing the processing tolerances of such long flexible cables.

6. Processing tolerances

The Kapton film is supplied by E. I. du Pont de Nemours & Co. in 30.5 × 30 480-cm rolls. It is expected to have a dielectric constant in the range of 3.3–3.5. While the manufacturer claimed a worst-case loss tangent of 0.0036, we measured a value of 0.008 (which is still relatively small). The line widths were measured both by cross sectioning and by observation from above with a high-magnification microscope. The width from the top was very uniform (±1%) along the entire 14.3-cm length, although the actual dimensions were about 7% higher than the nominal design values. The bottom widths showed a consistent narrowing that was much less predictable, and had at times a 30% variation along the length. Sample-to-sample reproducibility, however, was excellent. It should be pointed out that the microstrip design of our test structure represents an unsuitable condition for plating-based metallization. The line widths vary over a wide range, and the line separations are large. Uniform line widths and closer line separations are preferred in plating. In contrast, in the shielded-microstrip design of Figure 1(c), in which the lines are closer together and more uniformly packed, and which represents a more suitable condition for plating, the line-width uniformity was ±3.3%.

The Kapton thickness was uniform within ±4% over the entire area, and from sample to sample. The average signal-line thickness varied by only ±5%. However, the center portions of the lines tended to be as much as 14% thicker than the end dimensions. As can be seen from Figure 4, the covercoat layer of Kapton and the acrylic adhesive which is used to laminate it to the test structure have a nonplanar topography.

Because of difficulties in determining the exact line cross sections, the resistivity of the copper metallization was found to vary: namely, $\rho = 1.74$–2.09 μΩ-cm, with an average value $\rho_{avg} = 1.92$ μΩ-cm. This variation, however, is considered to be a reflection of dimensional tolerances and not of the metal itself.

7. Fastest signal propagation on flexible microstrip cable

Microstrip structures [Figure 1(b)] built on flexible films can propagate extremely fast rise-time signals. This was demonstrated by launching a 15-ps rise-time signal onto a 3.5-cm-long line which has a 75 × 25-μm cross section. Such a design was built with a signal line pitch of 0.3 mm (12 mils). The 6-ps step source from a 70-GHz sampling oscilloscope becomes a 15-ps transition at the interface between the probes and sample input pads. The signal at the end of the 3.5-cm-long line had a rise time of only 30 ps, which is the fastest propagation reported on such flexible connector structures; 60–100-ps rise times were measured on similar configurations in [22], but more common transitions are around 300 ps [5, 6]. In practical connector applications, where such a short length might be used, the section of flexible cable is not expected to be the limiting factor. The actual interface between the lines on the film and the transmission lines in the board or chip carrier are more likely to limit performance. They could consist of large pads and long vias, and have large, nonregular separations from the vias or pads connecting to ground planes. Such configurations arise because of the coarse ground rules that are currently feasible with printed circuit board or thick-film chip-carrier technology. The large capacitive and inductive discontinuities of these interfaces limit performance because of signal distortion and also contribute to reflected and coupled noise. Surface-mount connectors, with tight signal-to-ground spacings and 1:1 signal-to-ground allocations, can maintain

Table 2 Proposed triplate structure: Designs. Cross sections and calculated electrical characteristics of proposed cables with the triplate structure shown in Figure 1(d). The line widths W and thicknesses t are the same as the ones fabricated in the test vehicle and shown in Table 1. The Kapton thicknesses h_1, h_2 and pitch $W + S$ were chosen for Z_0 close to 50 Ω, and near-end coupled noise V_{NE} under 25 mV. These designs are used in the simulations shown in Figures 12 and 13.

W (μm) (mils)	S (μm) (mils)	t (μm) (mils)	h_1 (μm) (mils)	h_2 (μm) (mils)	*Pitch* (μm) (mils)	R (Ω/cm)	Z_0 (Ω)	V_{NE} (mV)
55.7 2.2	167.8 6.6	36.0 1.4	51.0 2.0	90.0 3.5	223.5 8.8	0.087	45.8	25.7
82.5 3.2	236.4 9.3	34.4 1.4	63.5 2.5	150.0 6.0	317.5 12.5	0.0624	46.9	20.3
161.3 6.4	346.7 13.6	36.0 1.4	126.3 5.0	200.0 7.9	508.0 20.0	0.03	47.0	19.9
212.8 8.4	422.2 16.6	36.3 1.4	166.7 6.6	254.0 10.0	635.0 25.0	0.0225	47.8	21.3

very good signal integrity. A less advanced interface which is more typical of actual applications is discussed in Section 9.

8. Maximum usable length for flexible triplate cables

In order to use flexible cables as high-performance interconnection media between widely separated parts of digital computer complexes, the triplate structure shown in Figure 1(d) must be adopted. This configuration creates an enclosed transmission line so that overlapping bundles of cables do not affect each other's characteristic impedance or generate additional crosstalk. Furthermore, energy loss through radiation is eliminated. The top Kapton layer and ground plane can be fabricated separately and then laminated to a structure of the type of Figure 1(b). This cross section tends to be less flexible, but sturdiness may, in fact, be desirable for long (1–2-m) spans.

Several cross sections were designed, with the restriction of maintaining a characteristic impedance around 50 Ω and a near-end coupled noise (V_{NE}) which is 2–2.5% of the input voltage swing. V_{NE} in this case is the saturated crosstalk, since the lengths of interest have delays longer than half the signal rise time. It is shown in [18] that V_{NE} is given by $(K_C + K_L)V_{in}/4$, where K_C is the capacitive coupling coefficient and K_L is the inductive coupling coefficient. The coupling coefficients are defined as the ratio of the mutual to self capacitance or inductance, respectively. The metal line widths were 55.7, 82.5, 161.3, and 212.8 μm (2.2, 3.2, 6.4, and 8.4 mil), and the metal thickness was assumed to be the same as that of the fabricated test structure (36.0 μm). The separation from the bottom ground, h_1, was selected to achieve the design objectives for Z_0 and V_{NE}. The top Kapton thickness, h_2, was chosen to produce only minimum reduction in Z_0, while the pitch, p $(W + S)$, was determined by the crosstalk budget. It is believed that this design is more likely to result in a reproducible cross section using standard flexible-film fabrication techniques than is a completely symmetrical strip-line. This is due to the proposed build sequence, where the top ground film must be laminated to the bottom structure. The resulting h_2 will always be thicker than h_1 because of the acrylic adhesive. Since the h_2 thickness affects the characteristics only marginally, its tolerance control is not critical. The cost is expected to be much lower than if a symmetrical strip-line structure were fabricated.

It should be noted, for example, that the same 82.5-μm (3.2-mil)-wide lines would have a 406.4-μm (16-mil) pitch in the case of the microstrip cross section of Figure 1(b), while the pitch can be reduced to 317.5 μm (12.5 mil) for the triplate design for the same V_{NE}. The triplate configuration helps achieve higher density and eliminates far-end coupled noise (V_{FE}) [18]. In the case of the coplanar waveguide structure of Figure 1(a), the same electrical characteristics can be achieved with a 304.8-μm (12-mil) pitch when ground conductors 134 μm wide (W_{GND} = 5.25 mil) are fabricated 45 μm (S = 1.77 mil) away from the signal lines. The range of line pitches was 223.5–635 μm (8.8–24 mil), and the line resistance was 0.0225–0.087 Ω/cm. The actual I/O density at the end of the cable is determined by the granularity of the fan-out lines and vias in the printed circuit board or chip carrier to which these films connect. The electrical performance is degraded at these interfaces if the cable density is not matched to board densities, as is discussed later.

The cross sections shown in **Table 2** were modeled with frequency-dependent losses, namely skin effect and dielectric dispersion with tan δ = 0.008. The propagation delay on these cables is of the order of 60 ps/cm, which would result in a delay of 6–15 ns for lengths of 100–250 cm. In digital applications where such cables could be used

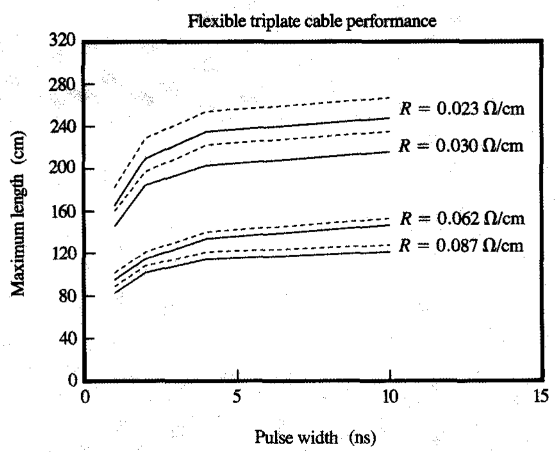

Figure 12

Calculated maximum useful lengths of flexible triplate cables [Figure 1(d)] as a function of transmitted pulse width, for lines of resistance R = 0.023–0.087 Ω/cm. The dashed lines correspond to a lossless (tan δ = 0.0) Kapton dielectric; the solid lines correspond to a dielectric with tan δ = 0.008. The designs considered are summarized in Table 2, while the results of this figure are summarized in Table 3. A voltage level of 600 mV at the output of the cables defines the maximum usable length when a pulse of 1 V amplitude is input to the cable.

instead of coaxial or optical interconnects, the propagation latency is not a performance-determining factor. What is important is to be able to transmit large bursts (blocks) of data with bit rates of the order of 100 Mb/s to 1 Gb/s. These transmissions usually employ a non-return-to-zero (NRZ) type of data detection which requires the distortionless propagation of 1–10-ns-wide pulses with small time jitter. One source of timing uncertainty can be a slow rise time crossing the receiver threshold; another is large variations in the characteristics of the connection medium. Frequency-dependent losses mostly attenuate the high-frequency components of the signals, which results in the rounding of the upper portion of a positive-going transition, as explained in [18]. Consequently, even for narrow pulses, the transition region through the switching threshold can be relatively unchanged, even for very long lengths.

A study was made of the maximum useful length for the four designs in Table 2, with pulse widths of 1, 2, 4, and 10 ns and a 1-V peak-to-peak (±0.5-V) amplitude, transmitted at clock rates of 2, 4, 8, and 20 ns, respectively. The driving signal had 200-ps rise and fall times. The requirement imposed at the output of the cable was that the time during which the voltage amplitude exceeded 300 mV (either positive or negative) must be at least half the input pulse width. This criterion was chosen as a relative indication of the maximum useful length for a particular cross section. For example, a typical bipolar receiver circuit would require about ±260-mV switching levels. Some extra margin was allowed, since the analysis carried out in this study considered only nominal conditions.

The results are tabulated in **Table 3** and plotted in **Figure 12** for both tan δ = 0 (dashed traces) and tan δ = 0.008 (solid traces). The dielectric dispersion reduces the maximum useful length by about 10 to 20 cm. The plots in Figure 12 show an increasingly large difference between the two cases as the lines become less resistive. This was expected, since dielectric loss tends to dominate over skin effect in the case of lines with smaller resistive losses. For pulse widths larger than about 4 ns, the maximum length is determined by the dc resistive drop. The decrease in rise times is a small fraction of the pulse width and will not

Table 3 Proposed triplate structure: Maximum useful lengths as a function of pulse width. Summary of calculated maximum useful lengths (cm) of flexible triplate cables [Figure 1(d)] for transmitted pulse widths of 1–10 ns. The modeling was done for the designs shown in Table 2 and the results are plotted in Figure 12. The input pulses had 1 V amplitude and 200 ps rise time. A level of 600 mV at the end of the cables defines the maximum useful length as described in the text. The results are shown both with (tan δ = 0.008) and without (tan δ = 0.0) dielectric loss.

R (Ω/cm)	*Maximum length* (cm)							
	10 ns pulse width		*4 ns pulse width*		*2 ns pulse width*		*1 ns pulse width*	
	tan δ = 0	*tan δ = 0.008*	*tan δ = 0*	*tan δ = 0.008*	*tan δ = 0*	*tan δ = 0.008*	*tan δ = 0*	*tan δ = 0.008*
0.0870	127.3	121.0	121.0	114.3	108.0	101.6	89.0	82.6
0.0624	152.7	146.4	140.0	133.7	121.0	114.3	101.6	95.3
0.030	235.0	216.0	222.3	203.0	197.0	184.0	160.0	145.8
0.0225	266.7	247.7	254.0	235.0	228.6	209.6	182.0	165.0

Z_0 = 46–48 Ω; V_{NE} = 20–26 mV.

affect the steady-state level significantly in this case. Because of resistive terminations that are used at the end of such cables, the dc current in the lines will cause a reduction in the steady-state level. However, as pulse widths become narrower, significant rounding of the upper and lower parts of the rise and fall times occurs because of skin effect and dielectric losses [18]. This rounding eats into the steady-state level and the time during which the voltage is greater than 300 mV, thereby limiting the maximum useful length. On the other hand, the pulse width itself, measured at the 50% level, does not change by much. For instance, the output rise and fall times for the 83-cm-long line with 55.7-μm-wide signal conductors increased to 350 ps, while the pulse width increased by only 35 ps. For a line 212.8 μm wide and 247.7 cm long, the output rise and fall times were 650 ps when a 10-ns-wide pulse was transmitted. The propagation delay measured at the 50% level increased only 2.7–4% due to dispersion.

Table 4 and **Figure 13** show the maximum length as a function of the bit rate, for the case of tan δ = 0.008. While 100 Mb/s can be transmitted on lines 121–247.7 cm long, 1 Gb/s can only be achieved for lengths of 82.6–165 cm. The longer lengths correspond to the wider lines with lower resistance. In **Figure 14** we show representative 1-Gb/s and 100-Mb/s responses for the shortest and longest line lengths, respectively, from Table 4.

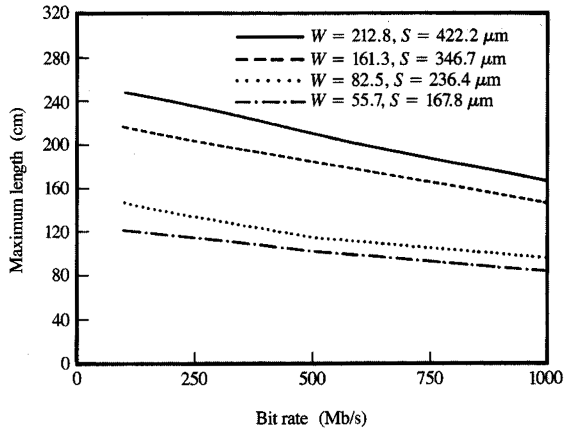

Figure 13

Calculated maximum usable length of flexible triplate cables [Figure 1(d)] for bit rates ranging from 100 Mb/s to 1 Gb/s. The widths W and separations S assumed in the calculation are shown in the inset. The wiring density range is 40–114 lines/in. Other assumptions include a characteristic impedance close to 50 Ω and near-end coupled noise under 25 mV for a 5-V/ns rise-time input signal. The results of this figure are summarized in Table 4. The inputs and criteria for maximum useful length are the same as those used in Figure 12.

9. Interface effects

A very important consideration in the use of flexible cables is the integrity of signal propagation at the interface between the film and the transmission lines in a multilayer printed circuit board or thick-film module. Such cables can be used to connect board to board, board to module, or module to module. A representative example is shown in **Figure 15** for board-to-multichip carrier connection. The film has pressure contacts which attach to surface pads on a 1.27 × 1.27-mm (50 × 50-mil) pitch at the board end and a 0.635 × 1.27-mm (25 × 50-mil) pitch at the module end.

Table 4 Proposed triplate structure: Maximum useful length as a function of bit rate. Summary of calculated maximum useful lengths (cm) of flexible triplate cables [Figure 1(d)] for bit rates of 100 Mb/s–1 Gb/s. The modeling was done for the designs of Table 2, with the same inputs and criteria for maximum usable length as were used in Table 3. The modeling results are plotted in Figure 13. Skin effect and dielectric loss (tan δ = 0.008) are both included.

Pitch (μm) (mils)	*W* (μm) (mils)	*S* (μm) (mils)	*Maximum length* (cm)			
			100 Mb/s bit rate	*250 Mb/s bit rate*	*500 Mb/s bit rate*	*1 Gb/s bit rate*
223.5 8.8	55.7 2.2	167.8 6.6	121.0	114.3	101.6	82.6
317.5 12.5	82.5 3.2	236.4 9.3	146.4	133.7	114.3	95.3
508.0 20.0	161.3 6.4	346.7 13.6	216.0	203.0	184.0	145.8
635.0 25.0	212.8 8.4	422.2 16.6	247.7	235.0	209.6	165.0

Z_0 = 46–48 Ω; V_{NE} = 20–26 mV.

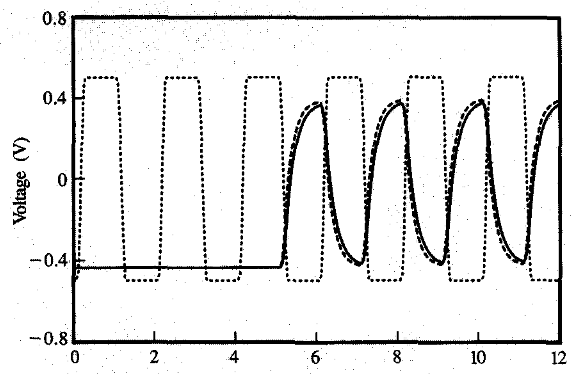

(a)

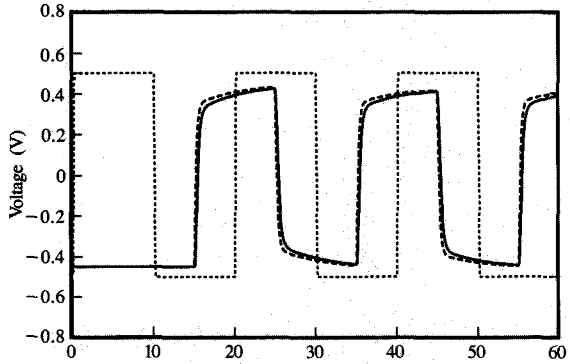

(b)

Figure 14

Simulated waveforms transmitted by two different representative triplate flexible cables from Table 4. In both cases the input pulses had a rise time of 200 ps and an amplitude of 1 V. The dotted line is the input waveform, the dashed line is simulated with a lossless dielectric (tan δ = 0.0), and the solid line is simulated with the measured loss tangent of tan δ = 0.008. (a) corresponds to an 82.5-cm-long cable with 55.7 μm (2.2-mil)-wide lines, with R_{dc} = 0.087 Ω/cm. A 1-Gb/s (1-ns pulses, 2-ns cycle time) application is considered. (b) corresponds to a 247.7-cm-long cable in a 100-Mb/s application (10-ns pulses, 20-ns cycle time). The transmission lines were 212.8 μm (8.4 mil) wide, with R_{dc} = 0.0225 Ω/cm.

The assignment of signal and ground pads can be quite irregular; a typical example with a 2:1 ratio is shown in **Figure 16(a)**. The lines on the film have a pitch of 211 μm (8.3 mil) and are 71 μm (2.8 mil) wide. The film cross section [**Figure 16(b)**] shows two types of voltage reference conductors which are 140 μm (5.5 mil) wide and have a 25.4-μm (1.0-mil) separation from the signal layer. This configuration, which is similar to a microstrip, allows signal referencing to be identical to the conditions used in the board or the carrier. The cross-sectional design is modeled precisely using the two-dimensional modeling program [18].

In this particular example, the film lines have a characteristic impedance of 46 Ω; the board lines have Z_0 = 58 Ω; the carrier has Z_0 = 55 Ω, with a fan-out layer having Z_0 = 40 Ω. Because of the coarse line widths and spaces available in typical board or thick-film carriers, the example of Figure 15 had to use four rows of contacts at the module end and eight rows at the board end, as shown in Figure 16(a). Figure 15 shows the layout of the signal layer. The connections from the flexible film to the signal lines in the two environments, board and module, are generally made through fairly long and large vias (of lengths V_1 and V_2) as shown in Figure 15. The resulting reference plane is relatively poor because of the large number of holes required for the vias. In addition, the coarse dimensions, which permit only low contact density and require many contact rows, cause an increase in the loop inductance for the current return.

The discontinuities in the contact area can generally be represented by lumped circuit elements because the delays through them are smaller than typical rise times (200–1000 ps). The signal rise time suffers minimal degradation at the interface. The inductive discontinuities, however, cause reflections which have amplitudes proportional to $[L/(2Z_0t_r)] \cdot V_{in}$, which can be significant. The actual reflected amplitude depends on the characteristic impedances of the transmission lines connected on either side of the connector, which in our example were quite different. Cleaner signals can be achieved using uniform characteristic impedances for the module, cable, connector, and board, but this may not be practical at a reasonable cost because of technological limitations. Alternatively, increasing the rise time would reduce the amplitude of the reflections at the discontinuity. However, slower signals reduce the system performance by preventing high bit-rate transmission. The loop inductances in the connector regions at the two ends of the flexible cable depend on the signal-to-ground contact ratio, and their spacing. Increasing the number of ground contacts without changing the contact spacings increases the number of contact rows and the overall size of the connector. The module end, with a finer grid of pads, and only four contact rows, clearly creates less distortion than the board end, which has a larger pad separation. The loop inductance at the board end, which includes the effect of the pads, vias, and connecting straps, was in the range of 4.2–6.5 nH, depending on the particular line modeled. The equivalent range for the module end was 3.0–4.3 nH. The corresponding capacitive discontinuities were 0.3–0.53 pF, and 0.28–0.44 pF, respectively. In this example, the flexible cable itself was 8 cm long.

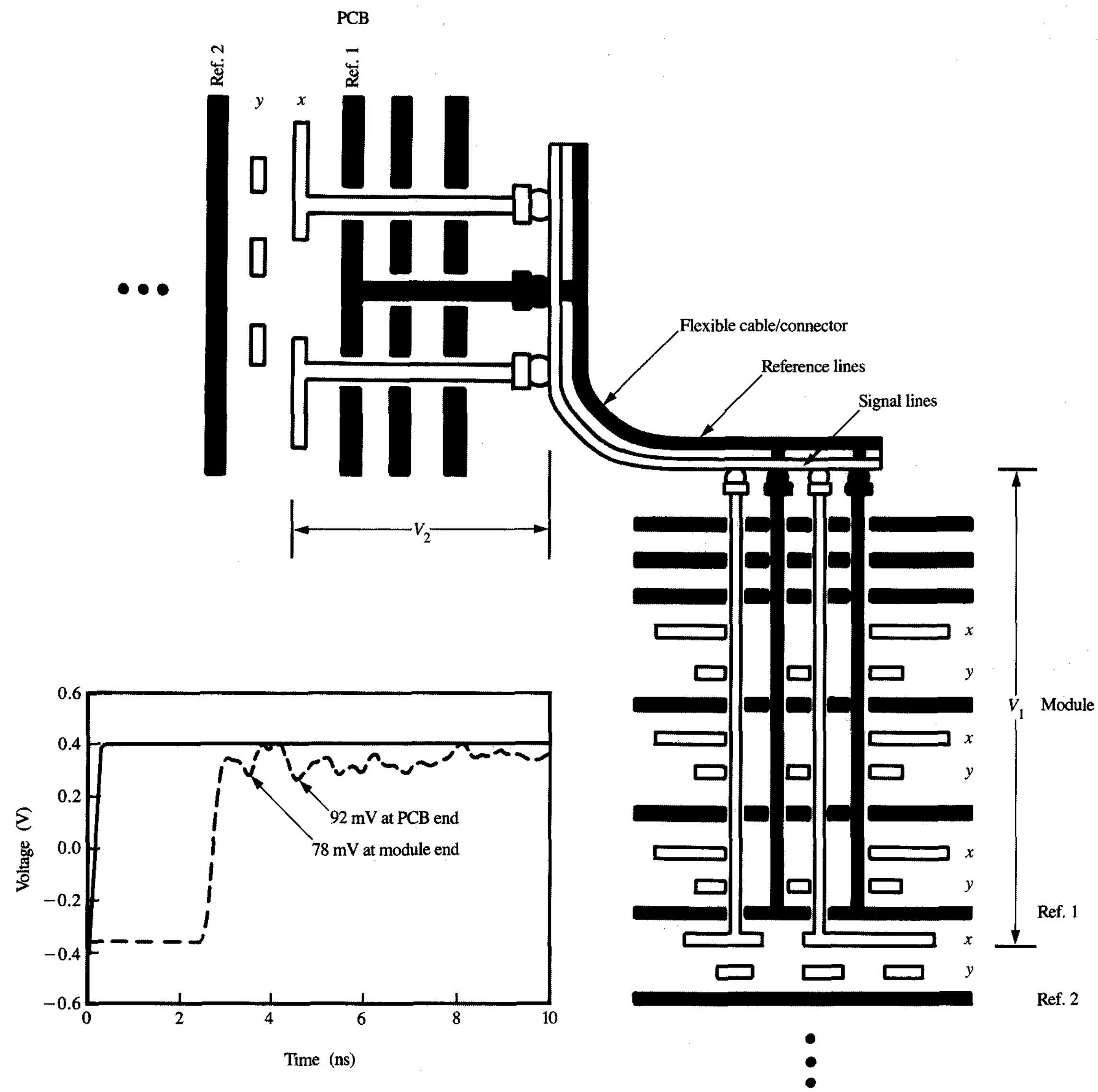

Figure 15

Representative flexible-film connector joining the signal lines in a chip carrier (module) and a printed circuit board (PCB). The diagram shows the discontinuities at the two contact regions. The transmission lines in the two carriers are at depths of V_1 and V_2 from the surface where the flexible cable is attached to the module and PCB, respectively. The inset shows a simulated transmitted waveform (dashed line) when a 200-ps-rise-time $\pm$400-mV signal (solid line) is input at the module end. The signal distortion due to discontinuities at the two ends is highlighted.

The inset in Figure 15 shows a representative simulated waveform observed at a receiver chip on the board following transmission of a 200-ps rise-time signal from a driver circuit on the module. The discontinuities from the transmission lines on the flexible cable to the transmission lines in the module and board were modeled as pi-networks with the lumped inductance and capacitance values given above. The reflections due to the two interfaces are clearly visible in this waveform. In this particular case, the reflected amplitude decreased from a worst-case value of 83 mV for a 3:1 signal-to-ground-pad ratio (S/G), to 42 mV for a 1:1 ratio. As expected, the

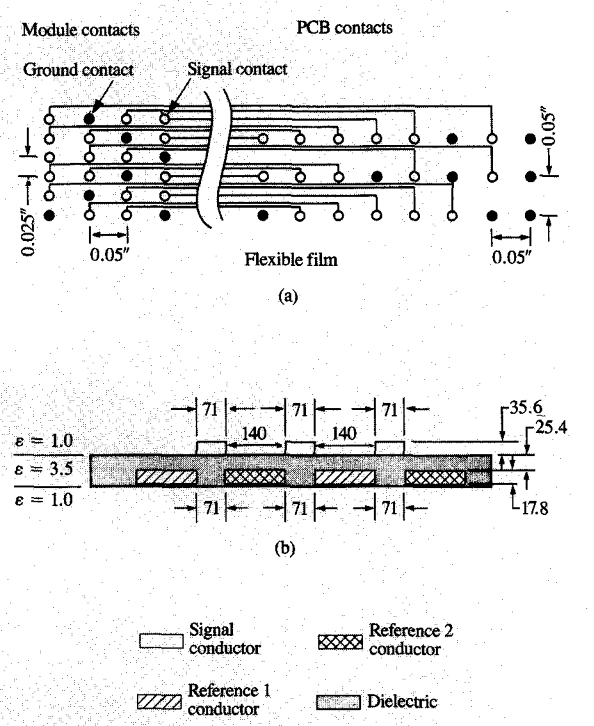

Figure 16

(a) Layout of a representative flexible-film connector showing typical signal and ground contact assignments at module (25 × 50-mil grid) and PCB (50 × 50-mil grid) interfaces. (b) Cross section of the flexible cable in the region between the end contacts. The 71-μm (2.8-mil)-wide lines are referenced to two separate voltages. The reference layer uses 140-μm (5.5-mil)-wide conductors. The line pitch is 211 μm (8.3 mil), and Z_0 = 46 Ω. This structure was input exactly into the modeling routines, though its behavior is similar to that of a microstrip design.

analysis showed a linear dependence of the reflected amplitude on the signal rise time.

Another factor limiting the rise time is the crosstalk generated at the interface area due to inductive coupling in the return contacts. Additional coupled noise is generated because of the nonuniform structure of the cable-to-board interface. This noise amplitude is inversely proportional to the signal rise time. Because of the short electrical length l in the interface area (compared with the signal rise time), the near-end coupled noise is proportional [18] to

$$V_{\mathrm{NE}} \cong K_{\mathrm{B}} 2\tau l V_{\mathrm{in}}/t_{\mathrm{r}}, \qquad (3)$$

where K_B is the backward-coupling coefficient explained earlier [$K_B = (K_C + K_L)/4$], and τ is the propagation delay. Typical capacitive (K_C) and inductive coupling (K_L) coefficients calculated for the example of Figures 15 and 16 were as follows. At the module interface, K_L = 0.1–0.31, K_C = 0.015–0.02; at the PCB interface, K_L = 0.26–0.4, K_C = 0.1–0.2. The contribution to overall crosstalk at the input to the receiver circuit, caused by the two connector interfaces, decreased from 61.3 mV to 42 mV when the driver rise time was reduced from 180 ps to 400 ps. The simulation considered two adjacent signal lines, one active and one quiet, with an excitation amplitude of 800 mV. The analysis shows that tighter contact and via spacings will significantly reduce the connector crosstalk.

10. Summary

We have experimentally characterized the electrical transmission properties of several flexible microstrip and shielded-microstrip cables. The results of our measurements were used to develop and refine models which describe their performance. On the basis of the knowledge gained, the use of these cables in high-performance applications was investigated. For instance, it was shown that existing microstrip flexible-film cables can transfer data at 1-Gb/s rates, with lengths of up to 83–165 cm, when the line widths are in the range of 55–212 μm. For a slower data rate of 100 Mb/s, microstrip line lengths of 121–248 cm are usable with the same dimensions. Dispersive effects are expected to introduce negligible timing uncertainty, since the latency on such cables is several ns. It was concluded from this study that in order to compete with discrete coaxial cables, flexible cables must use a shielded triplate structure. This configuration results in well-controlled transmission-line systems with a tighter pitch than microstrip designs, no radiation, no far-end-coupled noise, and infinite stacking capability. The challenge, however, is to fabricate 100–250-cm-long strips with good dimensional control. It is important to control the electrical performance of the flexible lines through tight tolerances, high density, and the use of low-loss polymers, in order to support the fast rise times and small timing uncertainty required for fast bit-rate transmission. The test structures used in this study had excellent dimensional tolerances along the length of the lines and also from sample to sample.

It was shown that the design and fabrication of the cables cannot be separated from the important issue of a high-performance connector. To achieve the 1-ns-wide pulses required by the 1-Gb/s bit rate, no significant additional distortion should be introduced at the connector. While the interface to printed circuit boards or chip carriers does not generally degrade the signal rise time, the large inductive and capacitive discontinuities introduced generate reflections and crosstalk noise that preclude the propagation of fast signals. An ideal interface should have a contact density commensurate with the film line density, 1:1 signal-to-ground contacts, short vias, surface-mount connections, and matched impedances throughout to minimize the effect of such discontinuities.

In conclusion, the key performance limits for flexible cables are processing tolerance for long lengths, dielectric loss, skin effect, and dc resistive drops on small-cross-section lines. In addition, triplate structures with tight via grids and high-density surface-mount interfaces are needed to interconnect future high-performance electronic packages.

Acknowledgments
The authors wish to thank R. D. Weale and his colleagues at IBM Endicott for their effort in fabricating for this study test samples with extremely good dimensional control.

References
1. *Microelectronics Packaging Handbook*, R. R. Tummala and E. J. Rymaszewski, Eds., Van Nostrand Reinhold, New York, 1989.
2. K. Ohno, K. Ohami, T. Takada, and G. Gotoh, "Fujitsu VP2000 System," *Nikkei Microdevices*, No. 48, pp. 42–49 (June 1989).
3. T. Watari and H. Murano, "Packaging Technology for the NEC SX Supercomputer," *IEEE Trans. Components, Hybrids, Manuf. Technol.* **CHMT-8**, 462–467 (1985).
4. R. Kaw, D. Yanaga, and F. Matta, "Multimetal DTAB Packages for a 125-MHz Computer," *Proceedings of the 42nd Electronic Components & Technology Conference, ECTC'92*, IEEE/EIA, San Diego, 1992, pp. 450–457.
5. T. Kon, K. Yasuda, and K. Nakano, "A New Printed Circuit Board Connector with Flexible Film Leads," *Proceedings of the 38th Electronic Components Conference, ECC'88*, IEEE/EIA, Los Angeles, 1988, pp. 220–225.
6. "AMP–ASC Interconnection Systems," *Product Information Bulletin 65188*, AMP Inc., Harrisburg, PA, February 1992.
7. F. Kobayashi, Y. Watanabe, M. Yamamoto, A. Anzai, A. Takahashi, T. Daikoku, and T. Fujita, "Hardware Technology for HITACHI M-880 Processor Group," *Proceedings of the 42nd Electronic Components & Technology Conference, ECTC'92*, IEEE/EIA, San Diego, 1992, pp. 693–703.
8. M. Yamada, M. Nishiyama, T. Tokaichi, and M. Okano, "Packaging Technology for the NEC ACOS System 3900," *Proceedings of the 42nd Electronic Components & Technology Conference, ECTC'92*, IEEE/EIA, San Diego, 1992, pp. 745–751.
9. G. Hansell and H. Vandeusen, "Interconnecting with Subminiature Digital Coax," *Proceedings of the 14th Annual Connector Symposium*, Electronic Connector Study Group, Camden, NJ, 1981, pp. 1–7.
10. *Gore-TEX Expanded PTFE Digital Signal Cable Specification Sheet, SIC 3201 for P.N. DXISN 1650-1*, W. L. Gore & Assoc., Inc., Elkton, MD, July 3, 1991.
11. S. Gazit, "Flexible Circuit Materials for Use as Interconnections in High Speed Digital Systems," *Proceedings of the 5th Annual International Electronics Packaging Conference*, IEEE, Orlando, FL, 1985, pp. 251–267; *Circuit World* **12**, 30–46 (1986).
12. C. Anderson, "Electrical Properties of an Input-Output Cable for Josephson Applications," *Rev. Sci. Instrum.* **53**, 1663–1666 (1982).
13. T. P. Russell, H. Gugger, and J. D. Swalen, "In-Plane Orientation of Polyimide," *J. Polymer Sci. Polymer Phys.* **21**, 1745–1756 (1983).
14. Y. Pastol, G. Arjavalingam, J.-M. Halbout, and G. V. Kopcsay, "Absorption and Dispersion of Low-Loss Dielectrics Measured with Microwave Transient Radiation," *Electron. Lett.* **25**, 523–524 (1989).
15. F. I. Shmabukuro and C. Yeh, "Attenuation Measurement of Very Low-Loss Dielectric Waveguides by the Cavity Resonator Method Applicable in the Millimeter/Submillimeter Wavelength Range," *IEEE Trans. Microwave Theor. Tech.* **36**, 1160–1166 (1988).
16. A. Deutsch, G. Arjavalingam, and G. V. Kopcsay, "Characterization of Resistive Transmission Lines by Short-Pulse Propagation," *IEEE Microwave & Guided Wave Lett.* **2**, 25–27 (1992).
17. V. A. Ranieri, A. Deutsch, G. V. Kopcsay, and G. Arjavalingam, "A Novel 24-GHz Bandwidth Coaxial Probe," *IEEE Trans. Instrum. & Meas.* **39**, 504–507 (1990).
18. A. Deutsch, G. V. Kopcsay, V. A. Ranieri, J. K. Cataldo, E. A. Galligan, W. S. Graham, R. P. McGouey, S. L. Nunes, J. R. Paraszczak, J. J. Ritsko, R. J. Serino, D. Y. Shih, and J. S. Wilczynski, "High-Speed Signal Propagation on Lossy Transmission Lines," *IBM J. Res. Develop.* **34**, 610–625 (1990).
19. W. T. Weeks, "Calculation of Coefficients of Capacitance of Multiconductor Transmission Lines in the Presence of a Dielectric Interface," *IEEE Trans. Microwave Theor. Tech.* **MTT-18**, 35–43 (1970).
20. W. T. Weeks, L. L. Wu, M. F. McAllister, and A. Singh, "Resistive and Inductive Skin Effect in Rectangular Conductors," *IBM J. Res. Develop.* **23**, 652–660 (1979).
21. *Advanced Statistical Analysis Program (ASTAP), Program Reference Manual*, Order No. SH20-1118-0; available through IBM branch offices; W. T. Weeks, A. J. Jimenez, G. W. Mahoney, D. Mehta, H. Qassemzadeh, and T. R. Scott, "Algorithms for ASTAP—A Network Analysis Program," *IEEE Trans. Circuit Theor.* **CT-20**, 628–634 (1973); A. J. Gruodis and C. S. Chang, "Coupled Lossy Transmission Line Characterization and Simulation," *IBM J. Res. Develop.* **25**, 25–41 (1981).
22. R. T. Smith and T. Chung, "High-Performance, High-Density Connectors Utilizing Multiple Layer Metal/Polymer Construction," *Proceedings of the 38th Electronic Components Conference, ECC'88*, IEEE/EIA, Los Angeles, 1988, pp. 226–233.

Received August 21, 1992; accepted for publication December 11, 1992

Alina Deutsch *IBM Research Division, P.O. Box 218, Yorktown Heights, New York 10598 (DEUTSCH at YKTVMV, deutsch@watson.ibm.com).* Mrs. Deutsch received the B.S. and M.S. degrees in electrical engineering from Columbia University and from Syracuse University, respectively. She has been at IBM since 1971 and has worked in several areas, including testing of semiconductor and magnetic bubble memory devices. She is a Senior Engineer currently working on the design, analysis, and measurement of package structures for future high-performance computer applications. Mrs. Deutsch has written many technical papers, holds six patents, and received an IBM Outstanding Technical Achievement Award in 1990. She is a member of Tau Beta Pi and Eta Kappa Nu, and a senior member of the IEEE.

David W. Dranchak *IBM Technology Products, 1701 North Street, Endicott, New York 13760 (DRANDW at ENDVMTKL).* Mr. Dranchak is a Staff Engineer in the Integrated Packaging Applications group at the Endicott Electronic Packaging Technology Laboratory. He received a B.M. degree in 1979 from Ithaca College, Ithaca, New York, and an M.S.E.E. degree in 1984 from the Georgia Institute of Technology, Atlanta. He joined IBM in July 1984. His work has been in various aspects of electronic packaging with emphasis on advanced technology connector development.

G. Arjavalingam *IBM Research Division, P.O. Box 218, Yorktown Heights, New York 10598 (ARJ at YKTVMV, arj@watson.ibm.com).* Dr. Arjavalingam received a B.A. degree from Cambridge University, U.K., in 1978, and M.S. and Ph.D. degrees from the University of California, Berkeley, in 1980 and 1983, respectively, all in electrical engineering. Since 1983 he has been at the IBM Thomas J. Watson Research Center, where he has worked on the amplification of ultraviolet subpicosecond pulses and various applications of short-pulse technology. Currently Dr. Arjavalingam is Manager of Package Design, Analysis, and Measurements at the IBM Research Division. He is a senior member of the IEEE and a member of the Optical Society of America.

Christopher W. Surovic *IBM Research Division, P.O. Box 218, Yorktown Heights, New York 10598 (CWS at YKTVMV).* Mr. Surovic is pursuing his associate degree in mechanical science and engineering at Westchester Community College. He has been at IBM since 1989 and has worked in the area of tool and model making for about four years, making significant contributions to the development of laser ablation tools and the Smithsonian X-Ray Telescope. Mr. Surovic is a Laboratory Technician currently working on electrical characterization of package structures for future computer applications. He has coauthored several technical papers in package measurements.

James K. Tam *IBM Research Division, P.O. Box 218, Yorktown Heights, New York 10598 (TAM at YKTVMV).* Mr. Tam received the B.S. and M.E. degrees in electrical engineering from Polytechnic University in 1984. He is pursuing his Ph.D. degree in the area of digital signal processing from the same university. He has been at IBM since 1984 and has worked in the area of chip design for high-performance computers for four years. Mr. Tam is a Senior Associate Engineer currently working on the design, analysis, and testing of package structures for future cost-performance computer applications. He has written several technical papers, holds one patent, and received an IBM Research Division Award in 1991.

Gerard V. Kopcsay *IBM Research Division, P.O. Box 218, Yorktown Heights, New York 10598 (KOPCSAY at YKTVMV, kopcsay@watson.ibm.com).* Mr. Kopcsay is a Research Staff Member in the Packaging Technology Department. His current research interests include measurement and analysis of high-speed pulse phenomena, and technology for high-performance computers. Since joining IBM Research in 1978, he has worked on the design and analysis of computer packages. He was manager of the Package Engineering Department from 1984 to 1988. Prior to joining IBM, he participated in research and development of low-noise microwave receivers at the AIL Division of Eaton Corporation. Mr. Kopcsay received the B.E. degree from Manhattan College in 1969, and the M.S. degree from the Polytechnic Institute of Brooklyn in 1974, both in electrical engineering. He is a member of the IEEE and the American Physical Society.

John B. Gillett *IBM Enterprise Systems, Kingston, New York 12401 (GILLETT at KGNVMX).* Mr. Gillett is a Senior Technical Staff Member with a B.S.E.E. degree from City University, London. He has been with IBM for 30 years, managing a wide variety of Advanced Technology programs. He holds 23 patents in the U.S., and a similar number abroad. His recent major activity has been in the packaging of high-performance computer systems, with particular interest in high-density interconnections, dense, high-current power supplies, and the organizational and technological impact of CMOS in high-performance computers. His present activity is developing new models for the prediction of solder-ball fatigue life for CMOS flip-chip packages.